

APPLICATION OF MESOSCALE FINITE ELEMENT SIMULATIONS TO STUDY THE EVOLUTION OF CUBE TEXTURE DURING HOT DEFORMATION OF ALUMINUM*

G.B. Sarma¹, B. Radhakrishnan¹, and T. Zacharia²

¹Computer Science and Mathematics Division

²Computing and Computational Sciences Directorate
Oak Ridge National Laboratory, Oak Ridge, TN 37831-6359, USA

Abstract

The origin and development of cube ($\{001\}\langle 100\rangle$) texture during hot deformation and subsequent recrystallization of aluminum alloys remains a topic of considerable interest in materials research. The application of finite element modeling at the mesoscale to study the hot deformation of microstructures containing cube oriented grains distributed among grains with S ($\{123\}\langle 634\rangle$) and copper ($\{112\}\langle 111\rangle$) orientations is described. Discretization of each grain with a large number of elements enables the model to capture the heterogeneous deformation of individual grains. The constitutive response of the material is modeled using crystal plasticity, thereby enabling the prediction of texture evolution in the microstructure. The deformation at elevated temperatures has been modeled by including slip on the non-octahedral $\{110\}\langle 110\rangle$ systems, in addition to the usual $\{111\}\langle 110\rangle$ systems. Microstructures with different grain sizes have been deformed in plane strain compression. The effects of the local environment, grain size and plastic strain on the stability of the cube texture during hot deformation are examined.

Introduction

The presence of cube texture in aluminum alloys subjected to thermomechanical processing under elevated temperature conditions is a topic that continues to receive considerable attention in materials research. The cube texture component is known to survive the hot deformation processing, and gain strength during subsequent annealing [1]. Under plane strain compression conditions, the activation of slip on non-octahedral systems $\{110\}\langle 110\rangle$ has been shown to lead to the stability of the cube component in aluminum alloys, both through experimental work and through modeling studies [2,3]. However, many of the experimental studies have involved single crystals or bi-crystals, and there has been less work to examine the effects of the microstructure on the stability of cube texture.

In this paper, the application of mesoscale finite element modeling to the deformations of microstructures containing cube-oriented grains distributed among other deformation components is described. The finite element discretization is applied at the grain level to model the inhomogeneous deformations of the microstructure. Crystal plasticity is used to model the constitutive response of the material, and hot deformation conditions are modeled by including slip on the $\{110\}\langle 110\rangle$ systems in addition to the usual $\{111\}\langle 110\rangle$ systems for fcc materials. Microstructures with relatively large and small grain sizes are considered, and some special

*The submitted manuscript has been authored by a contractor of the U.S. Government under contract No. DE-AC05-00OR22725. Accordingly, the U.S. Government retains a non-exclusive, royalty-free license to publish or reproduce the published form of this contribution, or allow others to do so, for U.S. Government purposes.

cases for the configuration of the cube-oriented regions are modeled. Deformation conditions approximating idealized plane strain compression have been used for the simulations to 75% reduction in height, and the effects of the immediate neighborhood, grain size and amount of plastic strain on the evolution of the cube oriented grains have been studied.

Mesoscale Deformation Model

The basic approach consists of discretizing a polycrystalline aggregate containing many grains using the finite element technique, often with many elements being employed to discretize each grain [4,5]. The microstructural state of the material is characterized by the orientation of the crystal lattice associated with each element relative to a fixed reference, and by the critical resolved shear stress parameter (strength) of the slip systems. The usual approach for distinguishing different grains in the microstructure is to assign the same initial orientation to all the elements comprising a grain. Grain boundaries are not modeled explicitly, but are assumed to exist between elements with different initial orientations. Compatibility between the different grains at the boundaries is satisfied implicitly through continuity in the velocity or displacement field. However, equilibrium in stress is achieved only globally in an approximate sense. The deformation of the discretized polycrystal is modeled through application of boundary conditions that usually approximate simple deformation conditions, such as tension, simple shear or plane strain compression. The simulations proceed incrementally, with the material microstructural state and geometry assumed to be unchanged while the velocity or displacement field is determined for a given strain increment. Balance laws for momentum and mass are used in conjunction with the material constitutive response to develop equations for the discretized velocity or displacement field. The resulting system of equations is non-linear and requires an iterative solution method. Following convergence of the displacement or velocity field, the material state and geometry are updated before proceeding to the next increment.

The plastic deformation of the material is assumed to occur predominantly by the movement of dislocations, which is typically restricted to specific directions on specific sets of atomic planes in the crystal. The dislocation motion is accompanied by interactions with other dislocations on different slip systems, causing an increase in resistance to further movement, and requiring a higher flow stress for continued plastic deformation (strain hardening). Due to the limited number of slip systems available to accommodate an arbitrary deformation, the crystal lattice has to rotate in order to maintain compatibility with the surrounding material.

The necessary mathematical framework to describe plastic deformation by slip is provided by crystal plasticity [6,7], which forms the basis for modeling constitutive behavior of the material. Based on Schmid's law, slip is assumed to commence when the shear stress resolved in the direction of slip on a given slip plane reaches a critical value τ_{cr}^{α} , which represents the strength of the slip system and parameterizes the resistance to dislocation motion. The relation between the applied stress σ and the resolved shear stress τ^{α} on a given slip system can be written using the Schmid orientation tensor (dyadic product of the slip direction s^{α} and slip plane normal vector n^{α}) as

$$\tau^{\alpha} = \sigma_{ij} n_j^{\alpha} s_i^{\alpha} = \sigma \cdot (s^{\alpha} \otimes n^{\alpha}) \quad (1)$$

The resolved shear stress τ^{α} is often related to the rate of shear $\dot{\gamma}^{\alpha}$ on each slip system through a power law,

$$\tau^\alpha = \tau_{cr} \frac{\dot{\gamma}^\alpha}{\dot{\gamma}_0} \left| \frac{\dot{\gamma}^\alpha}{\dot{\gamma}_0} \right|^{m-1} \quad (2)$$

where $\dot{\gamma}_0$ is the reference rate of shearing, and the exponent m represents the material strain rate sensitivity parameter. While the strengths of different slip systems can vary, lack of experimental data makes it difficult to characterize these differences, and hence the strength is assumed to be the same for all slip systems. Use of a rate dependent model allows for all slip systems to be potentially active, although the shear rates on some of them may be negligibly small, thus avoiding any ambiguities in the choice of the active slip systems. If the formulation is simplified to neglect elastic deformations, the crystal rate of deformation, which is the symmetric portion of the velocity gradient, can be written as a linear combination of the slip system shear rates,

$$\mathbf{D}_c = \sum_\alpha \mathbf{P}^\alpha \dot{\gamma}^\alpha \quad (3)$$

where \mathbf{P}^α is the symmetric part of the Schmid orientation tensor. Using equation (2) for the shear rate and equation (1) for the resolved shear stress, the above equation can be rewritten to develop a linearized constitutive relation for the crystal,

$$\mathbf{D}_c = \left[\sum_\alpha \left| \frac{\boldsymbol{\sigma} \cdot \mathbf{P}^\alpha}{\tau_{cr}} \right|^{\frac{1}{m}-1} \frac{\dot{\gamma}_0}{\tau_{cr}} \mathbf{P}^\alpha \otimes \mathbf{P}^\alpha \right] \boldsymbol{\sigma} \quad (4)$$

which can be solved to obtain the crystal stress for a given rate of deformation. The crystal spin \mathbf{W}_c is a combination of the plastic spin due to slip system shearing and any rigid rotation \mathbf{R}^* required to maintain compatibility with other crystals,

$$\mathbf{W}_c = \dot{\mathbf{R}}^* \mathbf{R}^{*T} + \sum_\alpha \mathbf{Q}^\alpha \dot{\gamma}^\alpha \quad (5)$$

where \mathbf{Q}^α is the skew-symmetric part of the Schmid orientation tensor. Equation (5) can be rewritten to obtain the rate of reorientation of the crystal, which in turn determines the texture evolution in the aggregate,

$$\dot{\mathbf{R}}^* = \left(\mathbf{W}_c - \sum_\alpha \mathbf{Q}^\alpha \dot{\gamma}^\alpha \right) \mathbf{R}^* \quad (6)$$

Strain hardening is modeled through an evolution equation for the critical resolved shear stress based on the accumulated shear rate on all slip systems,

$$\dot{\tau}_{cr} = H_0 \left(\frac{\tau_{cr}^s - \tau_{cr}}{\tau_{cr}^s - \tau_{cr}^0} \right) \sum_\beta |\dot{\gamma}^\beta| \quad (7)$$

where H_0 is the hardening rate, and τ_{cr}^0 and τ_{cr}^s are respectively the initial and the saturation values of the slip system critical resolved shear stress. The saturation value is computed using the accumulated shear rate as

$$\tau_{cr}^s = \tau_0^s \left(\frac{\sum_{\beta} |\dot{\gamma}^{\beta}|}{\dot{\gamma}_s} \right)^{m'} \quad (8)$$

where τ_0^s , $\dot{\gamma}_s$ and m' are material parameters. The rate sensitivity and other material parameters for the hardening equations are obtained by fitting the crystal plasticity model to experimentally measured stress-strain data.

As mentioned earlier, the increase in the slip system strength is a reflection of the increase in the dislocation density, which in turn may be related to the stored energy of deformation. For the purpose of subsequent recrystallization simulations using the output of the deformation modeling, the increase in stored energy of deformation per unit volume at each strain increment has been computed as the incremental work done,

$$\Delta \tau_{cr} \sum_{\beta} |\dot{\gamma}^{\beta}| \Delta t \quad (9)$$

The use of parallel computing tools has been of great advantage in applying the mesoscale deformation models to large three-dimensional discretizations. The iterative procedure for computing the velocity or displacement field during each strain increment requires repeated calculations of the element stiffness matrices, which in turn translates to solving the crystal plasticity equations many times. Low rate sensitivity values for metals, especially for room temperature deformation, lead to highly non-linear equations for developing the constitutive response. However, these calculations can proceed independently and simultaneously for the different elements in the mesh, making them efficient to perform on a parallel computer by distributing the computational load among many processors. Once the element stiffness matrices have been developed, they must be assembled to develop the global system of equations, and this step can be time consuming due to the need for exchange of data between the different processors. Efficient programs have been developed using the Message Passing Interface (MPI) libraries to minimize the time spent in this solution phase, leading to the capability to handle fairly large discretizations deformed to large plastic strains.

Simulations of deformation at the mesoscale

The mesoscale deformation model has been applied to microstructures containing cube oriented grains surrounded by other grains whose orientations were chosen to be variants of the ideal $\{123\}\langle 634 \rangle$ S and $\{112\}\langle 111 \rangle$ copper orientations. The finite element discretization used for each case consisted of a unit cube containing 40 hexahedral elements along each edge. Figure 1 shows an example of a typical discretized microstructure used in the simulations. The initial microstructures were generated using a Monte Carlo grain growth algorithm [8], which provided a lognormal grain size distribution. The grain orientations were randomly assigned as one of seven orientations—the ideal cube, the four variants of the ideal S orientation, and the two variants of the ideal copper orientation. Table 1 lists the various orientations used in the simulations. Two different microstructures containing 37 and 123 grains in a cubic grid of 40 sites along each side were chosen. For the microstructure with 37 grains, two of the grains were assigned the cube orientation, with the remaining grains being given one of the six other orientations. For the microstructure with 123 grains, the first 10 grain numbers were chosen to be cube, with the rest being distributed roughly equally among the six other orientations.

Table 1: Grain orientations used for the mesoscale hot deformation simulations.

Grain	{hkl}<uvw>	Euler angles
Cube	(0 0 1)[1 0 0]	(0,0,0)
S-1	(1 2 3)[-6 -3 4]	(31.02, 36.7, 63.43)
S-2	(1 2 -3)[6 3 4]	(-31.02, 143.3, 63.43)
S-3	(1 -2 3)[-6 -3 4]	(-31.02, 36.7, -63.43)
S-4	(1 -2 -3)[6 -3 4]	(31.02, 143.3, -63.43)
C-1	(1 1 2)[-1 -1 1]	(0, 35.26, 45)
C-2	(1 1 -2)[1 1 1]	(0, 144.74, 45)

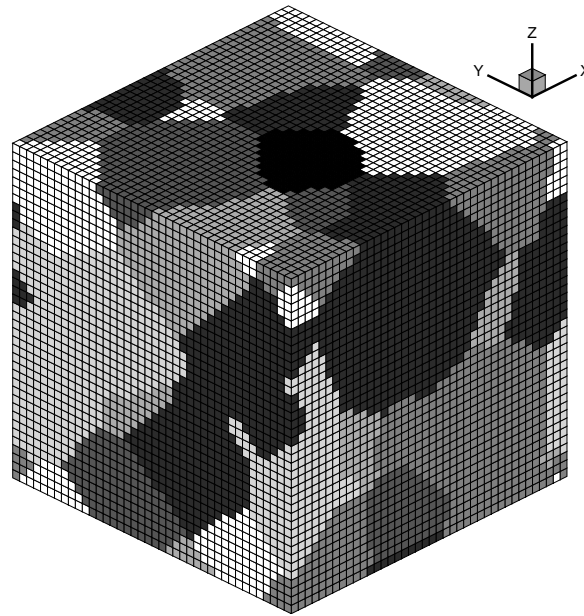


Figure 1: Discretized microstructure for the relatively large grain size.

In addition to the microstructures with the relatively large and small grains, three other microstructures were considered for the simulations. Each of these three cases was based on modifications to the microstructure with the 123 smaller grains, as described below. For each case, the orientations were chosen to be variants of S or copper, except for a zone in the middle that was chosen to be cube.

1. Cube-sphere: A spherical region of roughly 10 elements diameter in the middle was chosen to be at cube orientation.
2. Cube-block: A block of size 20×20×10 elements in the middle was chosen to be at cube orientation.
3. Cube-band: A zone of 10 elements thickness in the middle was assumed to be a single cube grain

Velocity boundary conditions that approximate ideal plane strain compression were prescribed in order to simulate the deformation. The normal velocity was set to zero for nodes on the bottom surface, while nodes on the top surface were given negative velocity that varied with

strain to maintain a constant overall strain rate. Nodes on the surface normal to $\pm Y$ were constrained to remain in plane with zero normal velocity, as were nodes on the surface normal to $-X$. In order to simulate large strains, nodes on the surface normal to $+X$ were also prescribed a velocity value with the same magnitude as the top surface, thus imposing an overall velocity gradient for ideal plane strain compression. The simulations were carried out using strain increments of 1%, and the results were examined after a reduction in height of 50% and 75%. Due to severe distortion of the elements, the simulations beyond 50% were carried out using a modified mesh generated by discretizing a parallelepiped that matched the overall dimensions of the domain after 50% reduction in height using $40 \times 40 \times 40$ regular elements of that aspect ratio. Figures 2 and 3 show the deformed microstructures for the large grain size after 50% and 75% reduction in height, respectively.

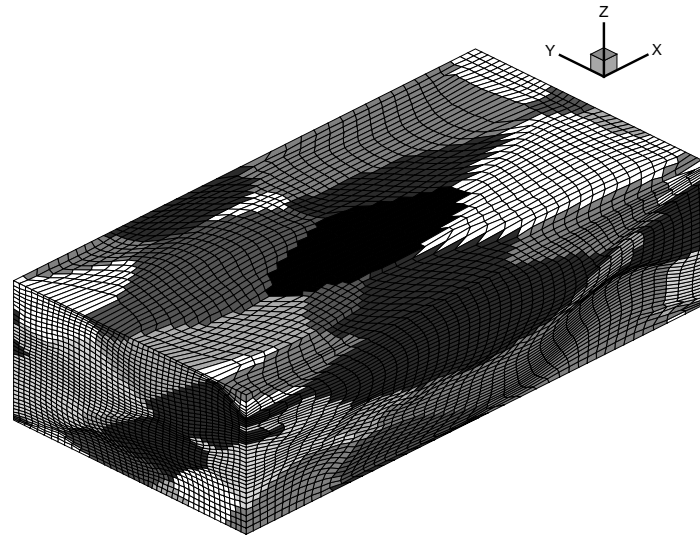


Figure 2: Deformed microstructures after 50% reduction in height for the microstructure with relatively large grain size.

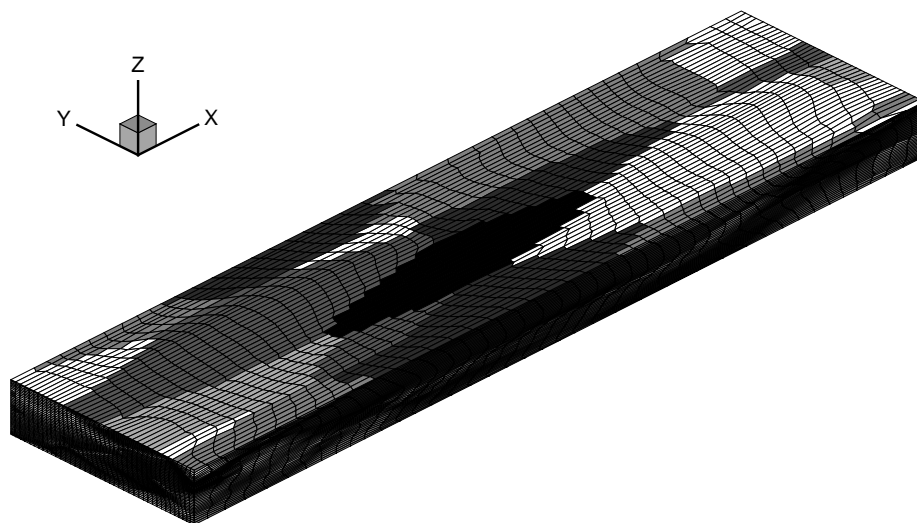


Figure 3: Deformed microstructures after 75% reduction in height for the microstructure with relatively large grain size.

The simulations were carried out for hot deformation conditions by assuming slip on the twelve $\{111\}\langle 110\rangle$ octahedral systems, and the six $\{110\}\langle 110\rangle$ non-octahedral systems. Material parameters for the crystal plasticity model were obtained using a polycrystal model to fit the stress-strain data from mechanical testing of 1100 aluminum at 400°C for various strain rates [9]. A random distribution of 1000 orientations was used for the fitting procedure, and the mechanical response was computed as the average response of the aggregate using the Taylor mean field hypothesis. The resulting values of the initial slip system strength, strain rate sensitivity and hardening parameters listed in Table 2 were used in the mesoscale modeling for the different microstructures considered.

Table 2: Material parameters used in the mesoscale hot deformation simulations.

m	$\dot{\gamma}_0$	H_0	τ_{cr}^0	τ_{cr}^s	$\dot{\gamma}_s$	m'
0.13	1.0 s ⁻¹	7.41 MPa	9.17 MPa	18.3 MPa	5×10 ¹⁰ s ⁻¹	0.01

Results and Discussion

In this section we present the results of the mesoscale simulations for the different microstructures deformed in plane strain compression under hot deformation conditions. For the case of the microstructures with large and small grain sizes, the results are presented for different 2-D sections in the XZ plane (i.e., the plane containing the “rolling” and “normal” directions). These sections were chosen in order to maximize the number of elements in the grains initially at cube orientation. For the microstructures with the cube-band, cube-block and cube-sphere zones, the results are presented for the mid-section. These sections were also the ones used in the subsequent simulations of recrystallization using the Monte Carlo technique, as described in detail elsewhere [10].

Figure 4 shows the deformed microstructure after a reduction in height by 50% for the section $j=17$ of the microstructure with relatively large grain size. The cube orientation is present near the top and bottom surfaces, and the neighboring grains are indicated in the figure. Also shown in Figure 4 are the contours of the stored energy of deformation, and the misorientation angle between the final and initial orientation for each element. The stored energy in the initially cube oriented grains is higher than in some neighboring grains. The stored energy is in general higher close to some of the boundaries between different grains, including a short and relatively flat stretch of the lower boundary of the cube grain near the top surface. The misorientation from the initial orientation for the cube grains is fairly low for elements away from the boundaries with neighboring grains. Near the boundary regions, however, the misorientation values are quite high, exceeding 45° in some cases. This trend continues with further deformation, as shown in Figure 5 after 75% reduction in height. Due to the high ratio of length to height, only a part of the domain along the extension direction containing the cube grain is shown. The stored energy values are higher in some regions of the cube grain compared to other grains, and the misorientation from the initial orientation is highest for elements near the boundary with the cube grain.

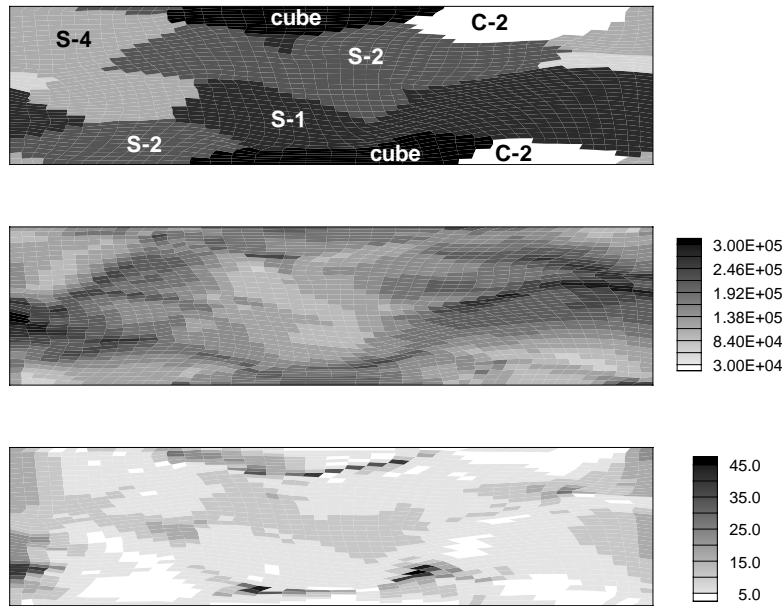


Figure 4: Deformed microstructure, stored energy [J/m^3] and misorientation [deg] from initial orientation for the microstructure with relatively large grain size, section $j=17$, after 50% reduction in height.

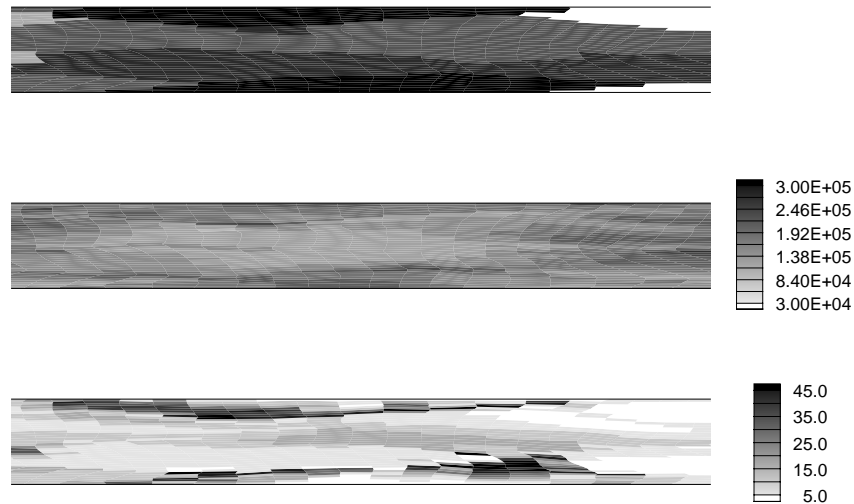


Figure 5: Deformed microstructure, stored energy [J/m^3] and misorientation [deg] from initial orientation for the microstructure with relatively large grain size, section $j=17$, after 75% reduction in height.

The deformed microstructure, stored energy distribution, and misorientation distribution for a different section ($j=25$) of the microstructure with large grain size are shown in Figures 6 and 7, respectively, for 50% and 75% deformation. The cube-oriented grain in this case is in the interior, surrounded by variants of the S orientation and the C-1 orientation. The stored energy in the cube grain shows variation from the left to the right side of the grain, and the misorientation is high in the vicinity of the boundaries between the cube grain and its neighboring grains. Note the energy difference along the boundary at the top of the cube grain, with lower stored energy on the cube side compared to the S-2 side. After 75% deformation, the trends remain similar to those seen after 50% deformation, with high misorientations close

to the cube grain boundaries. It is also observed that the misorientation along the top horizontal interface of the cube grain is low, whereas the misorientation values along the opposite side with inclined boundaries are quite high.

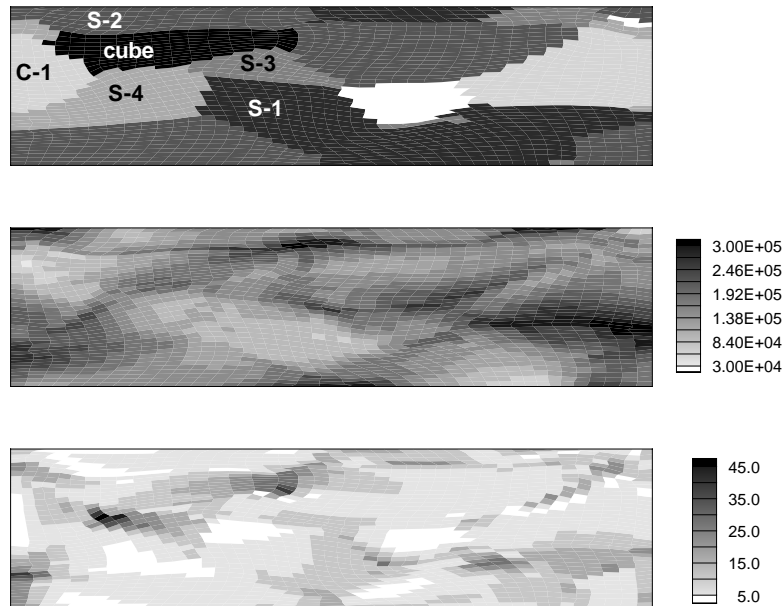


Figure 6: Deformed microstructure, stored energy [J/m^3] and misorientation [deg] from initial orientation for the microstructure with relatively large grain size, section $j=25$, after 50% reduction in height.

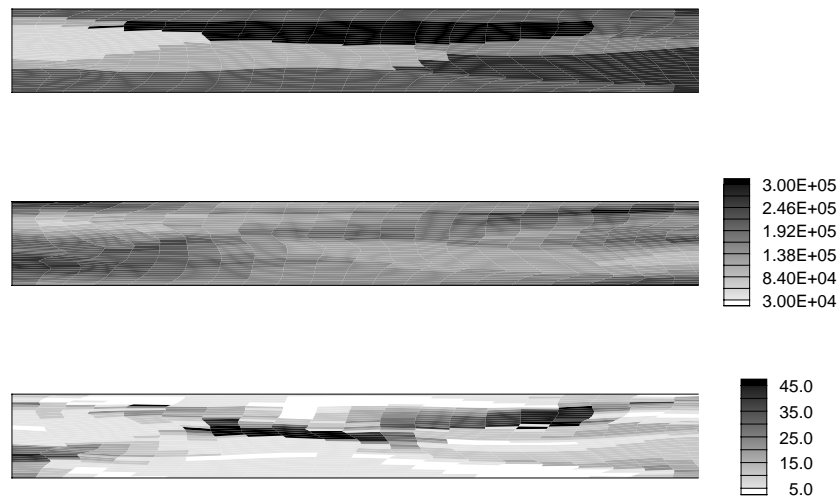


Figure 7: Deformed microstructure, stored energy [J/m^3] and misorientation [deg] from initial orientation for the microstructure with relatively large grain size, section $j=25$, after 75% reduction in height.

Simulations with a microstructure containing relatively small grain size showed similar overall results as compared to the microstructures with larger grains. Figure 8 shows the results for section $j=24$ after 50% deformation. This section contains cube grains near the top and bottom surfaces, and also a small interior grain. The misorientations from initial orientation are higher in the vicinity of the boundaries with the cube grain, indicating that these regions deform with larger reorientations compared to most other regions in the microstructure. The stored energy

of deformation in the cube grains is not uniformly low. The cube grain near the bottom surface has a relatively long flat interface with the neighboring C-2 grain, and the stored energy is high on the C-2 side along the interface. Such a difference is not evident along the other sections of the boundary. Similar results are seen after 75% deformation, as shown in Figure 9. For the cube grain near the bottom edge, the misorientation appears to be higher towards the left and right ends and much lower along the flat horizontal interface. Therefore, the orientation of the interface relative to the compression axis appears to have an effect on the amount of reorientation of the grains adjacent to the cube grains.

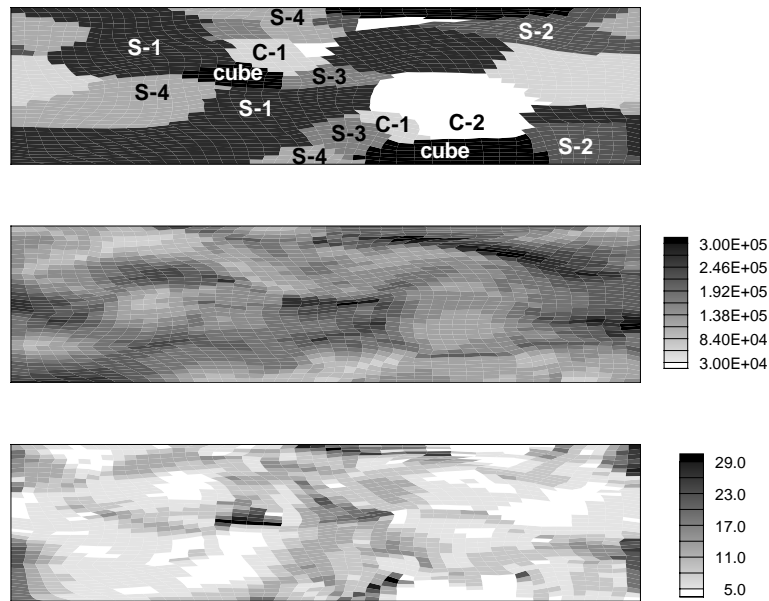


Figure 8: Deformed microstructure, stored energy [J/m³] and misorientation [deg] from initial orientation for the microstructure with relatively small grain size, section j=24, after 50% reduction in height.

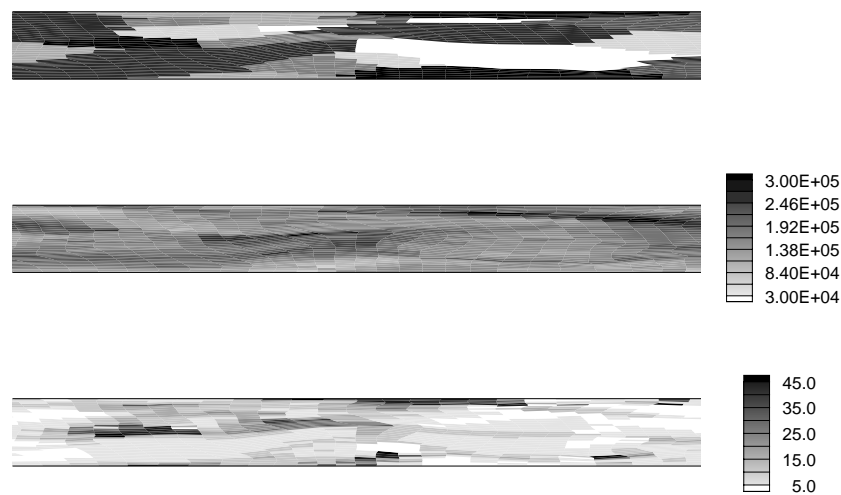


Figure 9: Deformed microstructure, stored energy [J/m³] and misorientation [deg] from initial orientation for the microstructure with relatively small grain size, section j=24, after 75% reduction in height.

Figures 10 and 11 show the results for the case of a roughly spherical cube grain at the center of the microstructure with small grain size after 50% and 75% deformation respectively. While the stored energy in the cube grain is not much lower than other regions, the misorientation from the initial orientation is lower in the interior of the cube grain. Once again, the cube grain shows variation in stored energy from left to right side, and lower values along the relatively flat interfaces, at the top with grain C-1, and at the bottom with grain S-1. For the regions adjacent to the cube boundary, the misorientation is higher at the left and right ends which have some vertical interfaces, compared to the central region which has a relatively flat interface in the horizontal direction.

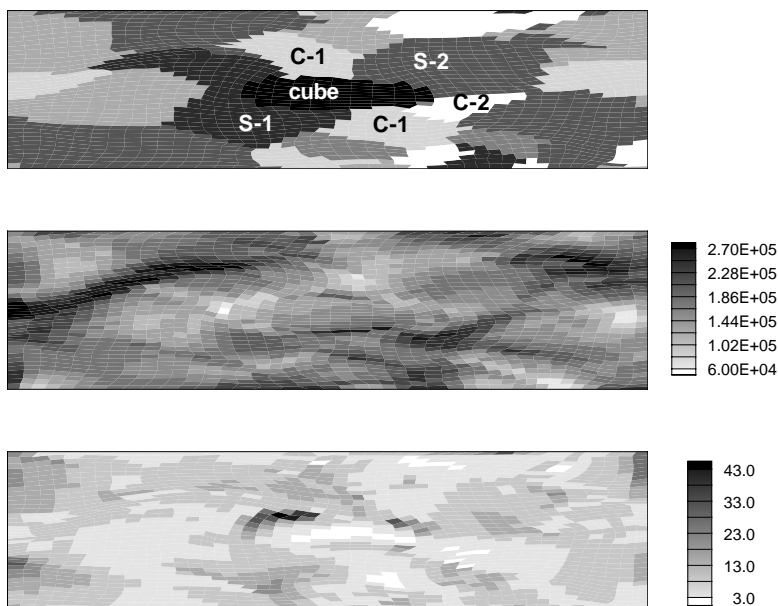


Figure 10: Deformed microstructure, stored energy [J/m^3] and misorientation [deg] from initial orientation for the microstructure with spherical cube grain at the mid-section after 50% reduction in height.

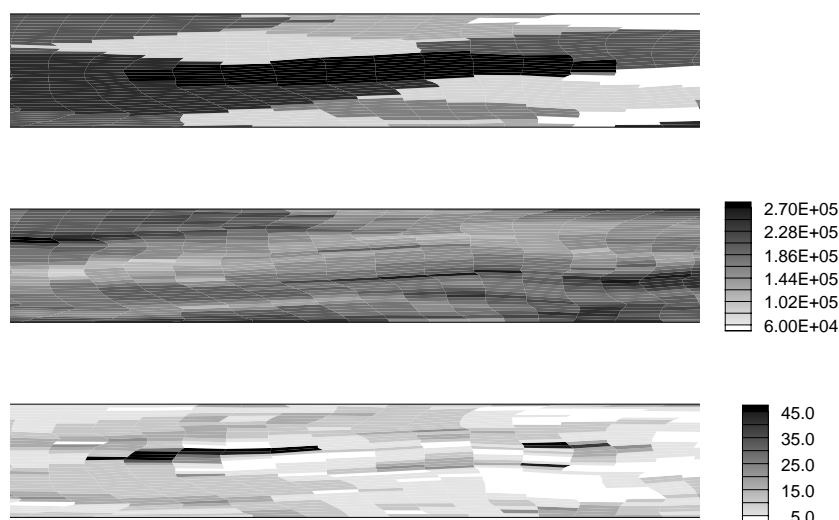


Figure 11: Deformed microstructure, stored energy [J/m^3] and misorientation [deg] from initial orientation for the microstructure with spherical cube grain at the mid-section after 75% reduction in height.

Figure 12 shows the results when the cube grain is now extended to form a sizeable block at the center of the microstructure, with a size of 20×10 for the section $j=20$ shown. The stored energy in the cube grain is lower than in the regions above and below, but this difference is less evident at the boundaries to the left and right side, and there are some grains to the left and right that have even lower values of energy. The misorientation distribution shows higher values near the boundaries with the cube grain, and as noted previously for the spherical cube grain, the misorientation is higher at the ends and fairly low along the flat interfaces. Similar results are obtained at higher strain after 75% deformation (Figure 13). As mentioned earlier, there seems to be a dependence on the shape of the cube grain interface on the reorientation of the adjacent S and copper grains during deformation.

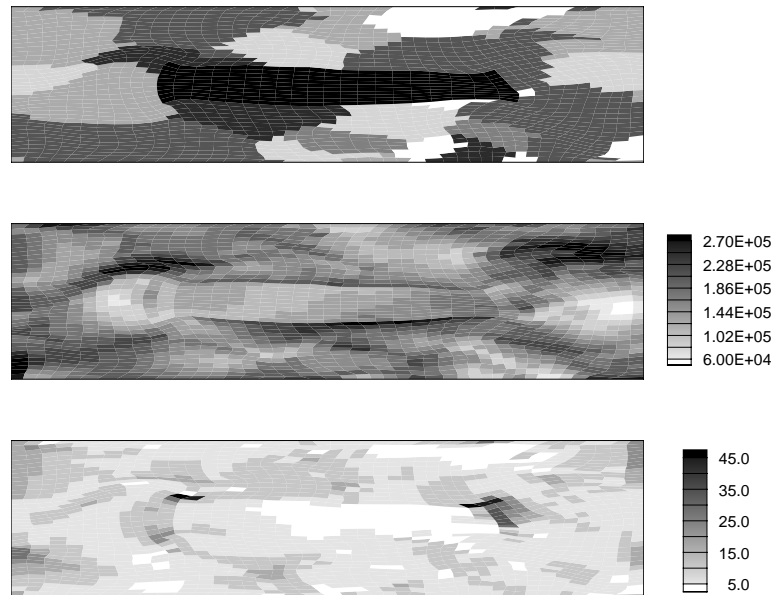


Figure 12: Deformed microstructure, stored energy [J/m^3] and misorientation [deg] from initial orientation for the microstructure with block-shaped cube grain at the mid-section after 50% reduction in height.

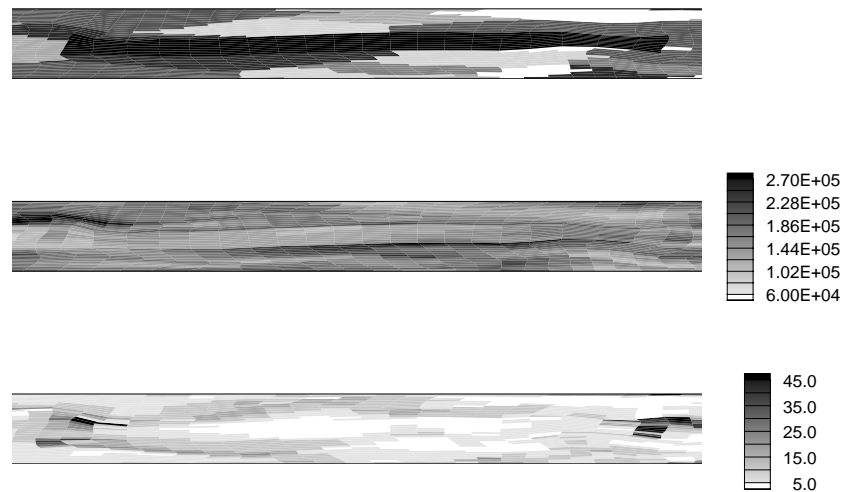


Figure 13: Deformed microstructure, stored energy [J/m^3] and misorientation [deg] from initial orientation for the microstructure with block-shaped cube grain at the mid-section after 75% reduction in height.

The case with the band of cube extending across the entire cross-section is a limiting case with only a flat interface with other grains. As shown in Figures 14 and 15 respectively for 50% and 75% deformation, the stored energy is lower in the cube grain compared to adjoining regions immediately above and below. The energy values are much lower in the central region compared to the ends, which are influenced to some extent by the boundary conditions to keep the surfaces flat. The misorientation values are also lower in the central region of the cube grain, and the boundary regions with the flat interface do not have very high misorientation values.

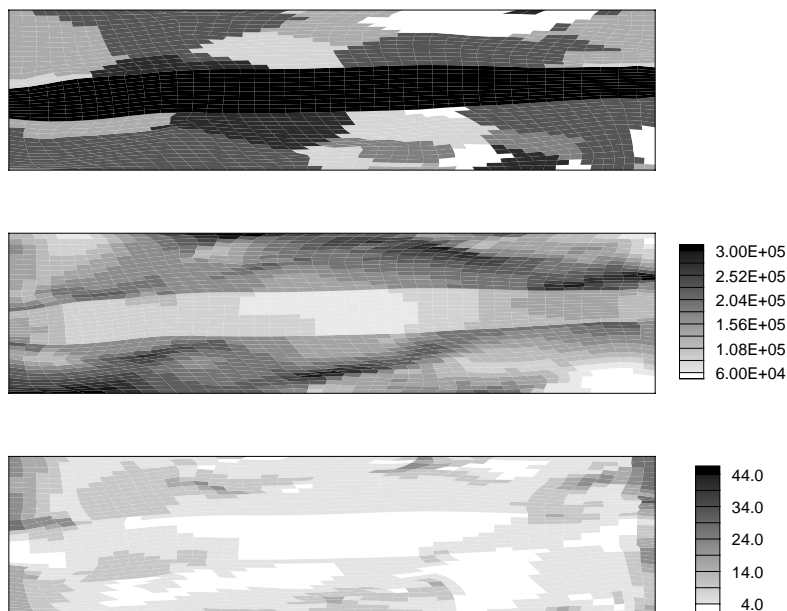


Figure 14: Deformed microstructure, stored energy [J/m^3] and misorientation [deg] from initial orientation for the microstructure with band-shaped cube grain at the mid-section after 50% reduction in height.

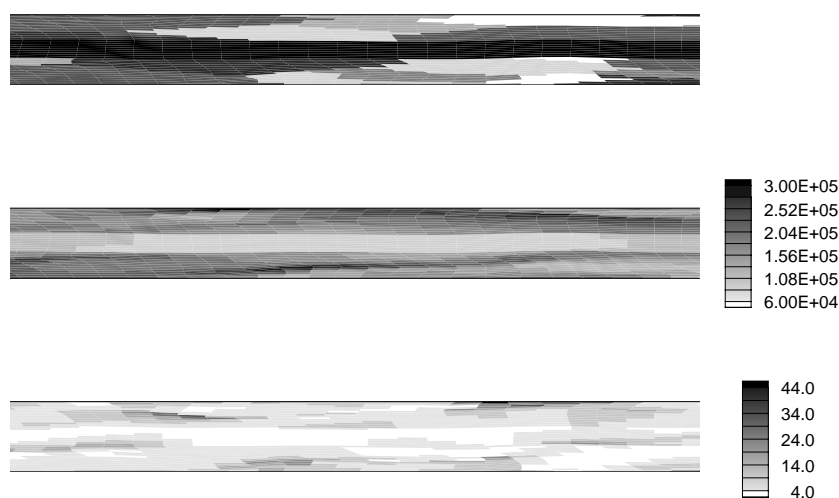


Figure 15: Deformed microstructure, stored energy [J/m^3] and misorientation [deg] from initial orientation for the microstructure with band-shaped cube grain at the mid-section after 75% reduction in height.

Conclusions

The application of mesoscale deformation modeling using the finite element method to study the evolution of microstructures containing cube oriented grains among grains with variants of the ideal S and copper orientations has been described. Use of a crystal plasticity model coupled with a hybrid finite element formulation has allowed the simulations to capture the inhomogeneous deformations at the level of individual grains due to the interactions with neighboring grains. Simulations with microstructures containing large and small grain sizes have been carried out, as well as some cases with specific configurations of the cube oriented regions. The microstructures have been deformed in plane strain compression under hot deformation condition by including possible slip on the $\{110\}\langle 110\rangle$ systems in addition to the usual $\{111\}\langle 110\rangle$ systems.

The results of the simulations have been examined mainly through the distributions of the stored energy of deformation and the misorientation from the initial orientation in the deformed microstructure. The stored energy values did not show a clear correlation with orientation, with cube-oriented grains not always showing the lowest values. A general trend related to the cube grain boundary shape was observed, with lower stored energy values on the cube grain side close the flat elongated boundaries parallel to the extension direction. This was particularly true for the case of a large block of cube and for the band of cube extending across the entire cross-section.

The approach used here for computing the stored energy based on equation (9) leads to values that are an order of magnitude larger than some recent experimental measurements based on single crystals [11]. The experimental values are based on measurements of the average subgrain size and subgrain misorientation in the deformed crystals, and the present model lacks sufficient detail to directly compute these quantities. Therefore, greater emphasis is placed on the relative differences between the stored energies at different locations, rather than on their absolute values.

The misorientation from the initial orientation is a measure of the extent of change in orientation as the material deforms. For all the cases examined, the misorientations were higher close to the boundaries between the cube and other orientations. The orientation of the interface relative to the loading axis was also observed to have an effect, with the elongated horizontal interface between the cube and other orientations showing low misorientations, whereas regions with a vertical or inclined interface showing the highest misorientations. The elongated flat interfaces also showed a difference in stored energy, with the energy being lower in the cube oriented region compared to the adjacent S or copper oriented region. Such regions are potential sites for the nucleation and growth of cube grains during subsequent annealing.

The amount of strain does not appear to have a significant effect on the microstructure evolution. The trends observed after 50% reduction in height in the distributions of stored energy and misorientation are not significantly altered after additional deformation to 75% reduction.

Acknowledgments

Research sponsored by the Office of Basic Energy Sciences, U.S. Department of Energy, under contract DE-AC05-00OR22725 with UT-Battelle, LLC. This research used resources of the Center for Computational Sciences at Oak Ridge National Laboratory, which is supported by the Office of Science of the U.S. Department of Energy, under contract DE-AC05-00OR22725.

References

1. O. Daaland, and E. Nes, "Origin of Cube Texture During Hot Rolling of Commercial Al-Mn-Mg Alloys," Acta Mater., 44 (4) (1996), 1389-1411.
2. Cl. Maurice, and J.H. Driver, "Hot Rolling Textures of f.c.c. Metals—Part I. Experimental Results on Al Single and Polycrystals," Acta Mater., 45 (12) (1997), 4627-4638.
3. G. Sarma, B. Radhakrishnan, and T. Zacharia, "Modelling the Deformation of Face Centered Cubic Crystals to Study the Effect of Slip on {110} Planes," Modelling Simul. Mater. Sci. Eng., 7 (1999), 1025-1043.
4. A.J. Beaudoin et al., "A Hybrid Finite-Element Formulation for Polycrystal Plasticity With Consideration of Macrostructural and Microstructural Linking," Int. J. Plast., 11 (5) (1995), 501-521.
5. G.B. Sarma, B. Radhakrishnan, and T. Zacharia, "Finite Element Simulations of Cold Deformation at the Mesoscale," Computational Material Science, 12 (2) (1998), 105-123.
6. R.J. Asaro, "Micromechanics of Crystals and Polycrystals," Adv. Appl. Mech., 23 (1983), 1-115.
7. R.J. Asaro, and A. Needleman, "Texture Development and Strain Hardening in Rate Dependent Polycrystals," Acta Mater., 33 (6) (1985), 923-953.
8. B. Radhakrishnan, and T. Zacharia, "Simulation of Curvature Driven Grain Growth by Using a Modified Monte-Carlo Algorithm," Metall. Mater. Trans., A26 (1) (1995), 167-180.
9. J.E. Hockett, "On Relating Flow Stress of Aluminum to Strain, Strain Rate, and Temperature," Trans. Metall. Soc. AIME, 239 (1967), 969-976.
10. B. Radhakrishnan, and G. Sarma, "Mesoscale Simulation of Cube Texture Evolution Following Hot Deformation of Aluminum," this volume.
11. M.C. Theyssier, and J.H. Driver, "Recrystallization Nucleation Mechanism Along Boundaries in Hot Deformed Al Bicrystals," Mater. Sci. Eng. A, 272 (1) (1999), 73-82.